Journal of Non-Crystalline Solids 492 (2018) 140–145

Contents lists available at ScienceDirect

Journal of Non-Crystalline Solids

journal homepage: www.elsevier.com/locate/jnoncrysol

The rheological behavior and thermoplastic deformation of Zr-based bulk metallic glasses

Chunyan Li[a,b,*], Fuping Zhu[a], Xiangyun Zhang[a], Juanqiang Ding[a], Jinfeng Yin[a], Zheng Wang[c], Yanchun Zhao[a,b], Shengzhong Kou[a,b]

[a] State Key Laboratory of Advanced Processing and Reuse of Nonferrous Metals, Lanzhou University of Technology, Lanzhou, Gansu 730050, People's Republic of China
[b] Wenzhou Engineering Institute of Pump & Valve, Lanzhou University of Technology, Wenzhou, Zhejiang 325000, People's Republic of China
[c] Sinotruk Group Jinan Truck Company Limited, Jinan, Shandong 250000, People's Republic of China

ARTICLE INFO

Keywords:
Rheological behavior
Processing map
The supercooled liquid region
High temperature compression
Hot processing

ABSTRACT

In this paper, the rheological behavior and thermoplastic deformation of $Zr_{61.88}Cu_{18}Ni_{10.12}Al_{10}$ bulk metallic glasses (BMGs) in the supercooled liquid region (SCLR) were studied by high temperature compression tests and a processing map was constructed. The results indicated that the flow stress of present alloy in the SCLR is very sensitive to temperature and strain-rate. The flow stress decreases with increasing temperature and decreasing strain-rate. The viscosity coefficient of the present alloy ranges from 10^{11} Pa.s to 10^{9} Pa.s and decreases with increasing temperature and strain-rate. When the strain-rate is greater than $5 \times 10^{-3}\,s^{-1}$, the $Zr_{61.88}Cu_{18}Ni_{10.12}Al_{10}$ alloy undergoes a transition from Newtonian fluid to non-Newtonian fluid. The surface profile exhibited a similar shape of the letter 'N' after high temperature compression in the deeply SCLR. The optimum hot processing region of $Zr_{61.88}Cu_{18}Ni_{10.12}Al_{10}$ alloy is 688 K–708 K with a low strain-rate and 708 K–723 K with a high strain-rate.

1. Introduction

The discovery of BMGs has triggered wide interest in academia [1]. Owing to the absence of long-range order and no crystal defects, BMGs have a series of attractive mechanical properties, for instance high strength, high hardness, oxidation resistance, corrosion resistance and small thermal expansion coefficient, etc. [2–9]. When the temperature reaches the SCLR, the viscosity coefficient of BMGs drops sharply with increasing temperature [10–12]. The feature of low viscosity coefficient in the SCLR contributes to thermoplastic forming (TPF) of BMGs [10]. This provides a new idea for the plastic processing of BMGs. It is found that the micro-parts made of BMGs have the advantages of high dimensional accuracy, excellent surface quality, high preparation efficiency and low costing comparing with the traditional crystal materials. BMGs are considered as a promising material for micro/nano-replication process [10]. Spaepen [8] firstly divided the plastic deformation of BMGs into two basic types: homogeneous plastic deformation and inhomogeneous plastic deformation. Previous works illustrated that the homogeneous plastic flow corresponds to Newtonian viscous flow that generally occurs at high temperature and low strain-rate [13–15].

2. Experimental procedure

Master alloy with nominal composition of $Zr_{61.88}Cu_{18}Ni_{10.12}Al_{10}$ was chosen for this study due to its excellent glass forming ability (GFA), large SCLR and good thermal stability [16,17]. The master alloy was prepared by levitation melting the constituent elements Zr, Cu, Ni and Al (purity ≈ 99.99%) under a high purity argon atmosphere. Master ingots were re-melted three times to ensure chemical homogeneity, followed by suction casting into a water-cooled copper mold in order to get rods with a diameter of 3 mm and a length of 70 mm. The amorphous structure of the master alloy was investigated by X-ray diffractometer (XRD, D/max-2400, Cu K_α). The thermal characteristic temperature of the BMGs were evaluated by differential scanning calorimeter (DSC, STA449) with a heating rate of 20 K/min, showing that T_g and T_x was 656 K and 750 K, respectively. It follows that the supercooled liquid region width $\Delta T_x = T_x - T_g = 94$ K.

Test specimens for high temperature compression tests, with a diameter of 3 mm and a length of 6 mm, were cut from the rods prepared in advance by a diamond slicer. High temperature compression tests were carried out using a Gleeble-3800 machine protected by high purity argon atmosphere. In order to explore the factors influencing the rheological behavior of the BMGs in the SCLR, various temperatures

* Corresponding author.
E-mail address: licywz@163.com (C. Li).

https://doi.org/10.1016/j.jnoncrysol.2018.04.026
Received 2 March 2018; Received in revised form 9 April 2018; Accepted 16 April 2018
Available online 24 April 2018
0022-3093/

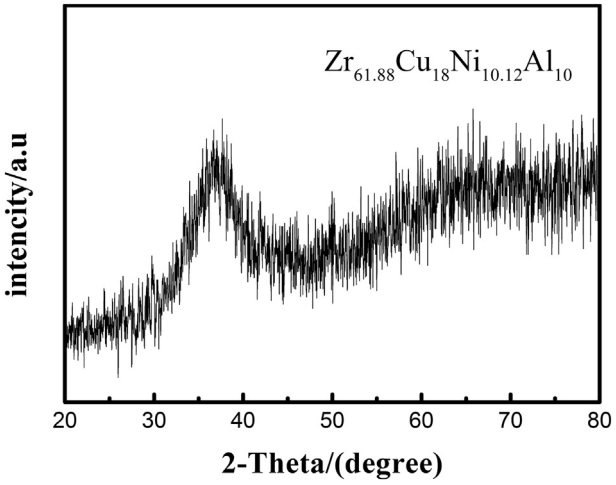

Fig. 1. XRD pattern of the as-cast $Zr_{61.88}Cu_{18}Ni_{10.12}Al_{10}$ specimen.

and strain-rates were selected (the temperatures and strain-rates are 678 K, 693 K, 708 K, 723 K, $10^{-2}s^{-1}$, $5 \times 10^{-3}s^{-1}$, $10^{-3}s^{-1}$, $5 \times 10^{-4}s^{-1}$ respectively). The surface morphology of the specimens after high temperature compression was observed by scanning electron microscopy (SEM, JSM-6700F). The high temperature compression tests were simulated using general finite element simulation software.

3. Results and discussion

Fig. 1 shows the XRD pattern of the as-cast $Zr_{61.88}Cu_{18}Ni_{10.12}Al_{10}$ specimen. It can be seen that the XRD pattern consists of one broad diffuse peak between diffraction angles 30°and 45°. It indicates that the master alloy has a perfect glassy structure.

Figs. 2–3 illustrated the compression stress-strain curves of $Zr_{61.88}Cu_{18}Ni_{10.12}Al_{10}$ glassy alloy under different deformation condition in the SCLR. It can be seen from Figs. 2–3 that the deformation temperature and strain rate have a significant effect on the plastic rheological behavior of the BMGs in the SCLR. At first, it can clearly observed the occurrence of elastic deformation during high temperature compression tests, followed by a stress "over-shoot" phenomenon, then the flow stress gradually stabilized [18]. According to the "free volume theory", due to the existence of free volume, the BMGs are not completely tight stacking state. According to Refs [8], the plastic deformation of the BMGs in the SCLR is accomplished by the creation and annihilation of free volume. When the deformation temperature and strain-rate are low, owing to the low activation energy, it is not enough to provide enough free volume for atomic transition, resulting in the stress sharply increases to form peak stress. And then the peak stress works, so that the atoms squeeze into smaller space, resulting in the generation of new free volume, which continues to support the atomic transition, hence the stress decreases and tends to be gentle [8].

It can be clearly seen from Fig. 2 that the stress peak gradually increases with increasing strain-rates, as is shown in Fig. 2(a)–(d). The flow stress is considered as the peak-stress in order to eliminate the elastic contribution [19]. When the strain-rate is lower than $5 \times 10^{-3}s^{-1}$, the flow stress occur distinct decline, as is shown in Fig. 2(b)–(c). This phenomenon indicates that present alloy is sensitive to applied strain-rates. The flow stress-strain curves in Fig. 2(c) exhibit good regularity and the flow stress is low. Especially, when the strain-rates are $10^{-3}s^{-1}$ and $5 \times 10^{-4}s^{-1}$, the curves do not display obvious stress "over-shoot" phenomenon, indicating that the plastic deformation is more stable. At this time, alloy specimens show Newtonian fluid characteristics. Owing to the lower strain rate, resulting that the heating time is too long, the specimens may generate nano-crystalline during the high temperature compression process [19]. The dispersive distribution of the nano-crystalline plays a crucial role in dispersion strengthening that further hinder the flow of the flow units, resulting in a suddenly rise of the flow stress, as is shown in Fig. 2(d).

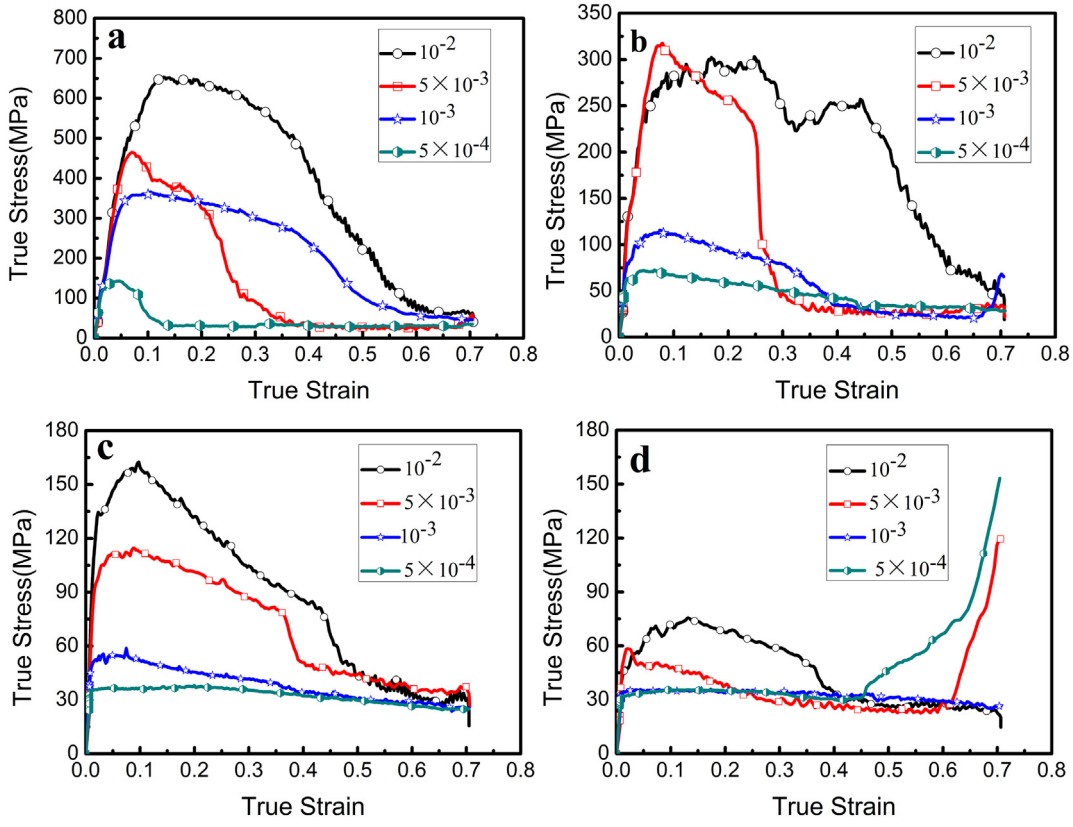

Fig. 2. Compression stress-strain curves of $Zr_{61.88}Cu_{18}Ni_{10.12}Al_{10}$ specimens at different strain-rates.

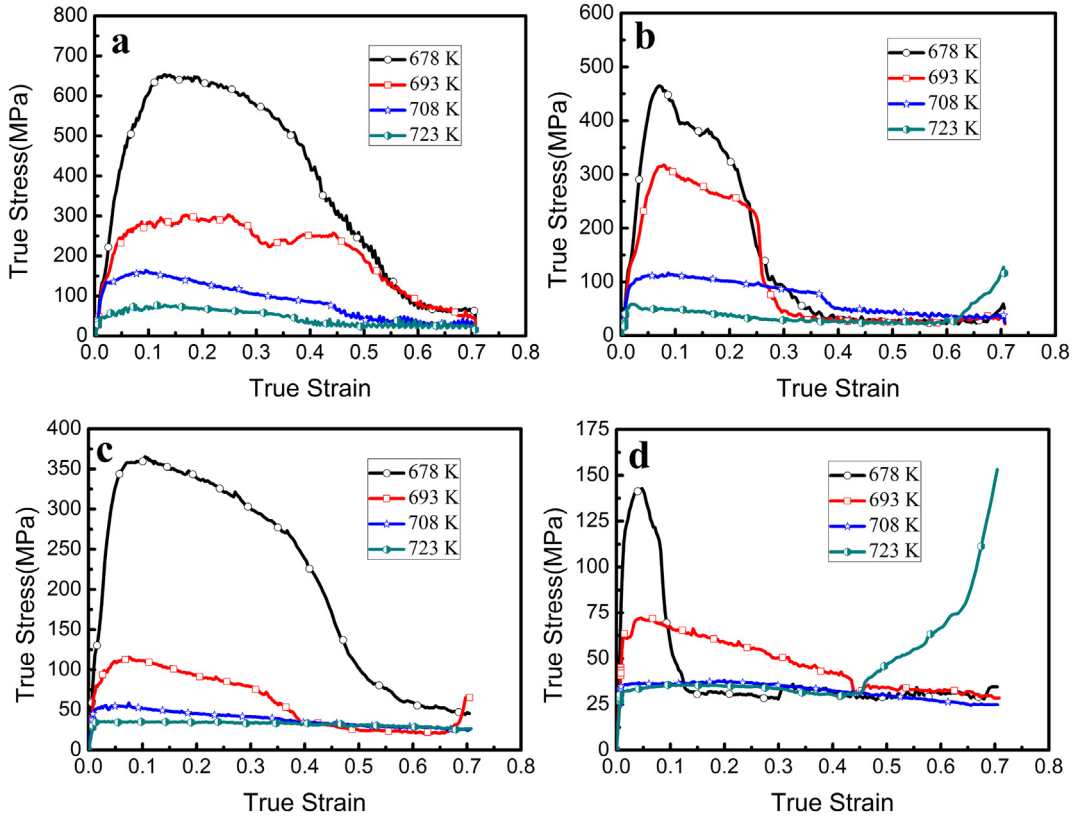

Fig. 3. Compression stress-strain curves of $Zr_{61.88}Cu_{18}Ni_{10.12}Al_{10}$ alloy at different temperatures.

The impact of temperature on the stress-strain relationship of specimens was exhibited in Fig. 3. AVD Beukel [20] believes that the amount of free volume varies with temperature and the amount of free volume increases with increasing temperature. As the temperature increases, the amount of free volume increases, plastic deformation by free volume creation and annihilation becomes easier and the resistance of the alloy to external deformation becomes smaller, so that the stress overshoot gradually disappears, as is exhibited in Fig. 3(a)–(d). Especially, When the temperature is higher than 693 K, the flow stress appears obvious decline and occurs the phenomenon of strain increases but the stress almost does not increase (Newtonian viscous fluid characteristics), as is shown in Fig. 3(a)–(c). This phenomenon indicates that present alloy is very sensitive to temperature. Owing to the incubation time of crystallization is shortened at high temperature, the specimens may generate nano-crystalline during the high temperature compression process. As a result, there is a work hardening phenomenon due to the impact of the dispersion strengthening aroused by nano-crystalline, as is shown in Fig. 3(d).

The relationship between the flow stress and strain-rate of $Zr_{61.88}Cu_{18}Ni_{10.12}Al_{10}$ alloy is exhibited in Fig. 4(a). The flow stress of specimens ranges from 653 MPa (appears at 678 K with a strain-rate of $10^{-2}\,s^{-1}$) to 33 MPa (appears at 723 K with a strain-rate of $5 \times 10^{-4}\,s^{-1}$). The flow stress of specimens decreases with increasing temperature and decreasing strain-rate. When the temperature reaches 708 K and 723 K, the flow stress of specimen is lower than the other temperatures and flow stress and strain rate have a good linear relationship. W.H. Wang [21] believes that the stress and the strain-rate of the material are linear in the Newtonian deformation zone. We can observe from Fig. 4(a), the stress and the strain-rate are linear at 708 K. So at that time, the BMGs belong to Newtonian fluid. According to the logarithmic relationship of Backofen function [22].

$$\lg\sigma = m\lg\dot{\varepsilon} + \lg K \tag{1}$$

where σ_{flow} is the flow stress, K is a constant, $\dot{\varepsilon}$ is the strain-rate and m is the strain rate sensitivity exponent. So the slope of the flow stress-strain rate curves reflects the strain-rate sensitivity exponent. It can be observed that when the strain-rate is greater than $5 \times 10^{-3}\,s^{-1}$ ($\lg(0.005) \approx -2.3$), the slope of the curves decreases indicating that the specimens undergo a transition from Newtonian fluids to non-Newtonian fluids.

It is well known that viscosity coefficient is an indispensable parameter describing the flow behavior of BMGs in the SCLR. One of the differences between Newtonian and non-Newtonian fluids is whether the viscosity coefficient is a constant. According to the conventional equation

$$\eta = \sigma_{flow}/3\dot{\varepsilon} \tag{2}$$

the viscosity coefficients of the material at various temperatures and strain-rates were calculated and summarized in Table 1. Furthermore, strain-rate dependence of viscosity coefficient for specimens was plotted in Fig. 4(b). It can be clearly observed that the viscosity coefficient ranges from 10^{11} Pa·s at 678 K (near T_g) to 10^{9} Pa·s at 723 K (close to T_x). The viscosity coefficient decreases with increasing strain-rates. This phenomenon shows that the present alloy undergo a transition from Newtonian flow at low strain-rates to non-Newtonian flow at high strain-rates. Especially, when the test temperature is greater than 693 K, the variation of the viscosity coefficient with strain-rate is small and the alloy specimens show uniform plastic deformation (Newtonian viscous fluid characteristics). At this time, the BMGs belong to Newtonian fluid. Combined with flow stress-strain curves of Fig. 2(c), it can be found that the flow behavior of $Zr_{61.88}Cu_{18}Ni_{10.12}Al_{10}$ alloy is relatively stable at 708 K, which belongs to the typical Newtonian rheological state and is very favorable for TPF.

Temperature as another major factor affected the flow properties of BMGs in the SCLR plays an indispensable role in the rheological process of the material. According to Table 1, the change regularity of viscosity coefficient with temperature was analyzed, as shown in Fig. 4(c). In general, the viscosity coefficient of specimens do not vary linearly with

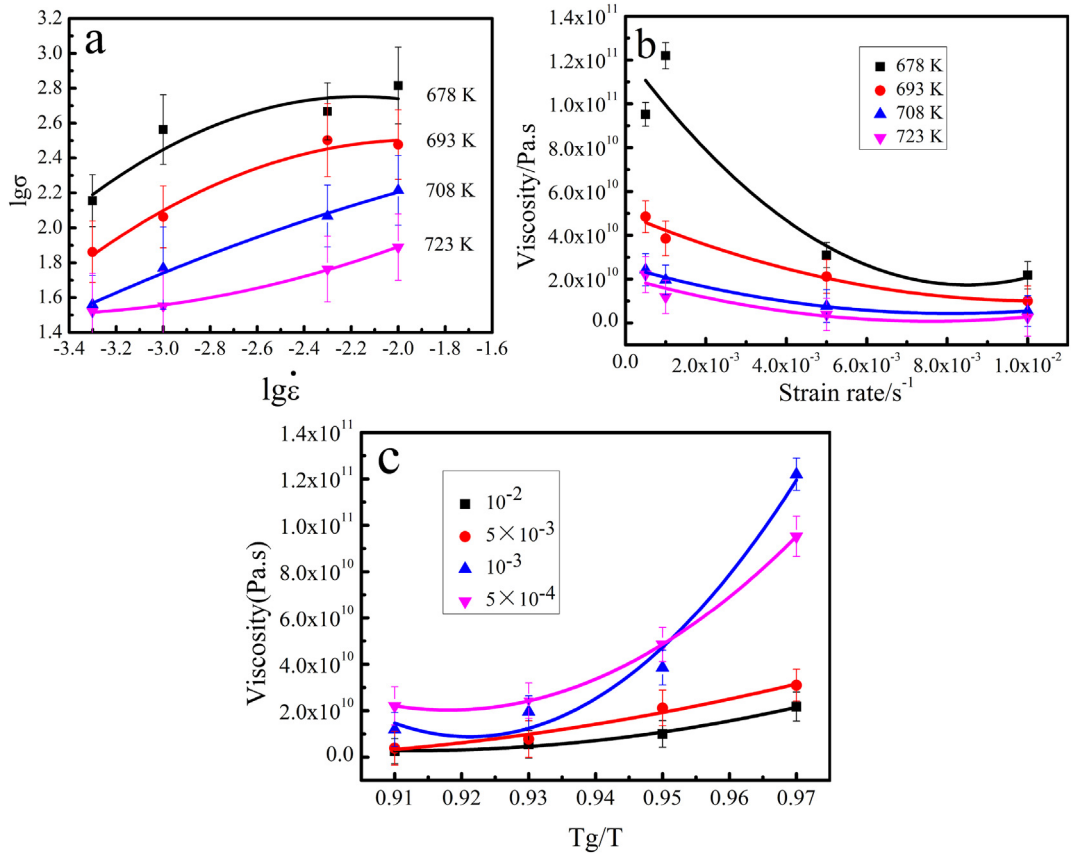

Fig. 4. The relationship between logarithm stress-logarithm strain rate (a); Viscosity changes with strain rate (b) and temperature (c).

Table 1
Viscosity coefficient of $Zr_{61.88}Cu_{18}Ni_{10.12}Al_{10}$ alloy at different temperatures and strain-rates ($\times 10^{10}$ Pa·s).

Strain-rate(s^{-1})	678 K	693 K	708 K	723 K
$5 \times 10^{-4} s^{-1}$	9.5 ± 0.22	4.9 ± 0.27	2.4 ± 0.25	2.2 ± 0.38
$10^{-3} s^{-1}$	12 ± 0.16	3.9 ± 0.14	1.9 ± 0.2	1.2 ± 0.16
$5 \times 10^{-3} s^{-1}$	3.0 ± 0.02	2.1 ± 0.04	0.78 ± 0.03	0.39 ± 0.03
$10^{-2} s^{-1}$	2.2 ± 0.01	1.0 ± 0.02	0.55 ± 0.01	0.26 ± 0.02

temperature, it decreases with increasing temperature and reaches a minimum of 2.6×10^9 Pa·s at 723 K with a strain-rate of $10^{-2} s^{-1}$. Especially, when the strain-rate is greater than $5 \times 10^{-3} s^{-1}$, the alloy specimens also exhibit high rheological behavior. The result is similar to the experimental result of Wang [23].

In addition, due to errors of the measurement accuracy of experimental equipment such as thermocouples and sensors during the experiment, there are different deviations of the experimental data. Through the multiple tests and the error analysis of the experimental data, the standard deviation of the data is obtained. The error bar of the experimental data was plotted, as is shown in Fig. 4.

Fig. 5 shows the surface profile's low magnification SEM images of the specimens after high temperature compression tests, the surface profile at 678 K with a strain-rate of $10^{-2} s^{-1}$ is exhibited in Fig. 5(a). It can be clearly observed that the tested specimen exhibits a similar shape of the letter 'N' as a whole at low temperature with a high strain-rate and there are many folds on the surface of the tested specimen. It may be related to the interaction between the shear bond and the stress along the axial direction of the specimen. Fig. 5(b) shows the surface profile of the tested specimen at 693 K with a strain-rate of $5 \times 10^{-3} s^{-1}$. Comparing with Fig. 5(a), the surface is smoother. In addition, the 'N'-type profile disappeared and transformed to a shape which is similar to drum. This phenomenon can be explained that as the temperature increases, plastic deformation by free volume creation and annihilation becomes easier and the resistance of the alloy to external deformation becomes smaller. The transformation of these two shapes means that the alloy specimens undergo a process from non-uniform to uniform rheology.

In order to analyze the flow status and stress-strain relationship of the specimens in the SCLR, the flow status of the material in the process of high temperature compression tests are simulated by the general finite element software and compared with the experimental data, the result is shown in Fig. 6. The simulation result and experimental result are exhibited in Fig. 6(a) and (c). According to the simulation result, the stress-strain curve of the material was plotted and compared with the experimental results, as is shown in Fig. 6(d). It is found that the simulation result and experimental result are very closer. The finite element software was used to simulate the flow velocity change of the test specimen during the compression process. It was found that the flow velocity of the material at the stress end is faster than the other end and the flow velocity of the intermediate part is between the two ends. Perhaps this is one of the reasons why the test specimen is compressed into a drum-like shape, as shown in Fig. 6(b).

"Processability" is a significant index to measure the ability of metal plastic forming. The processability of metal materials contains two aspects: the inherent processability and the impact of stress state. There is a rheological instability phenomenon in the process of high temperature compression tests and there is a safety zone and a destabilization zone. The establishment of processing map can enable us to analyze and simulate the process of metal plastic molding and master the impact of various process parameters on the material flow process, so as to control the microstructure evolution and optimize the process parameters [24]. Based on the dynamic material model (DMM) [25], the rheological instability criterion proposed by Murty [26] and the numerical

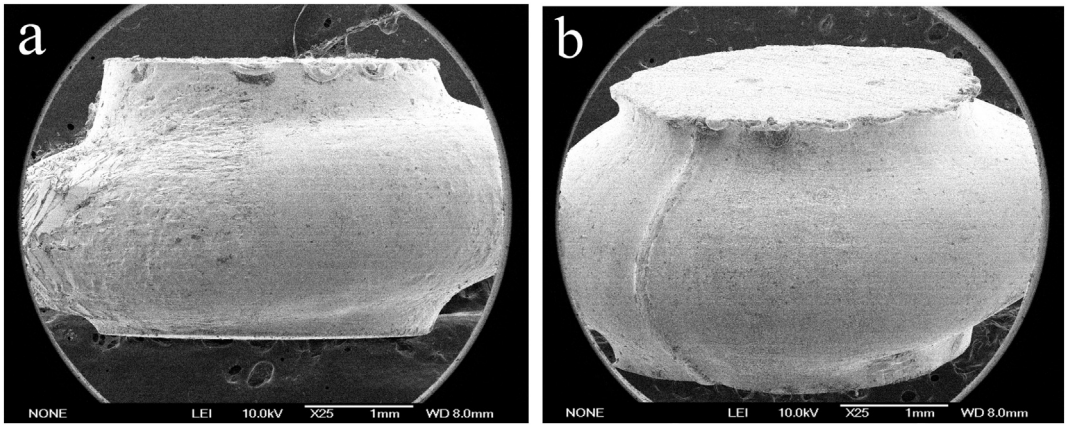

Fig. 5. Surface profile of the $Zr_{61.88}Cu_{18}Ni_{10.12}Al_{10}$ alloys after high temperature compression tests, (a) 678 K-10^{-2} s^{-1}; (b) 693 K-5 × 10^{-3} s^{-1}.

structure method of Jun Zhou [24] are used. The flow state of the test specimens in the SCLR was analyzed by MATLAB software. The results are shown in Fig. 6. Usually we believe that the superplastic area is the area that the energy dissipation efficiency is more than 60%. Fig. 7(a) shows the energy dissipation diagram which can observe from Fig. 7(a) that the energy dissipation efficiency is less than 60% consist of two parts, one part is the region with low-temperature and high strain-rate, the other part is the region with high-temperature and intermediate strain-rate. The energy dissipation efficiency of the alloy in the other temperature region is about 60%–80%, which belongs to the superplastic region.

The reason of rheological instability is that the rate of system generates entropy does not match the rate of external entropy applied to the system. Fig. 7(b) shows the rheological instability diagram. It is found that the unstable region mainly includes two parts, one part is the low-temperature region with a high strain-rate and the other part is the high-temperature region with a low strain-rate. Compared with the energy dissipation diagram and the rheological instability diagram, it can be concluded that the optimum hot processing region of $Zr_{61.88}Cu_{18}Ni_{10.12}Al_{10}$ alloy is 688 K–708 K with a low strain-rate and 708 K–723 K with a high strain-rate.

4. Conclusions

The main findings of this study are:

(1) The flow stress of $Zr_{61.88}Cu_{18}Ni_{10.12}Al_{10}$ alloy is sensitive to temperature and strain-rate. The flow stress decreases with increasing temperature and decreasing strain-rate. When the strain-rate is greater than 5 × 10^{-3} s^{-1}, the $Zr_{61.88}Cu_{18}Ni_{10.12}Al_{10}$ alloy undergoes a transition from Newtonian fluids to non-Newtonian fluids. In addition, the test temperature is greater than 693 K, the $Zr_{61.88}Cu_{18}Ni_{10.12}Al_{10}$ alloy presents Newtonian viscous fluid characteristics.

(2) The viscosity coefficient of $Zr_{61.88}Cu_{18}Ni_{10.12}Al_{10}$ alloy ranged from 10^{11} Pa·s to 10^{9} Pa·s and exhibited a tendency to decrease with increasing temperature and strain-rate.

(3) According to the results of SEM, it can be find that the specimens

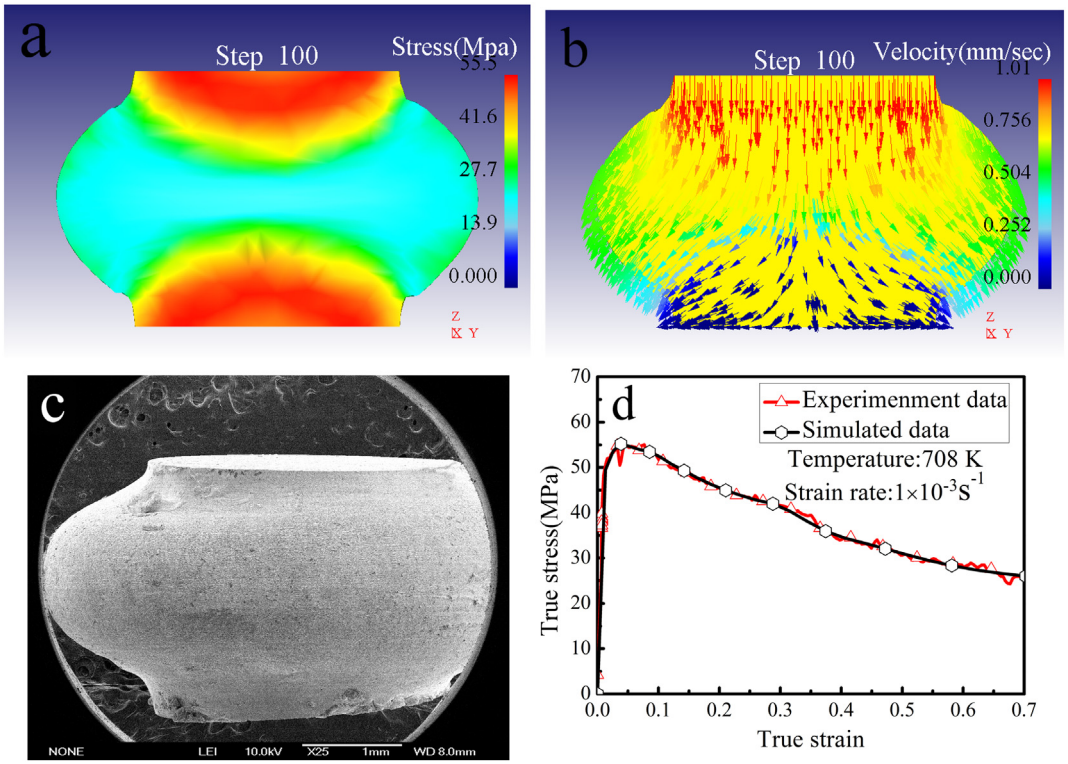

Fig. 6. Finite element simulation results of $Zr_{61.88}Cu_{18}Ni_{10.12}Al_{10}$ alloy compressed in the supercooled liquid region.

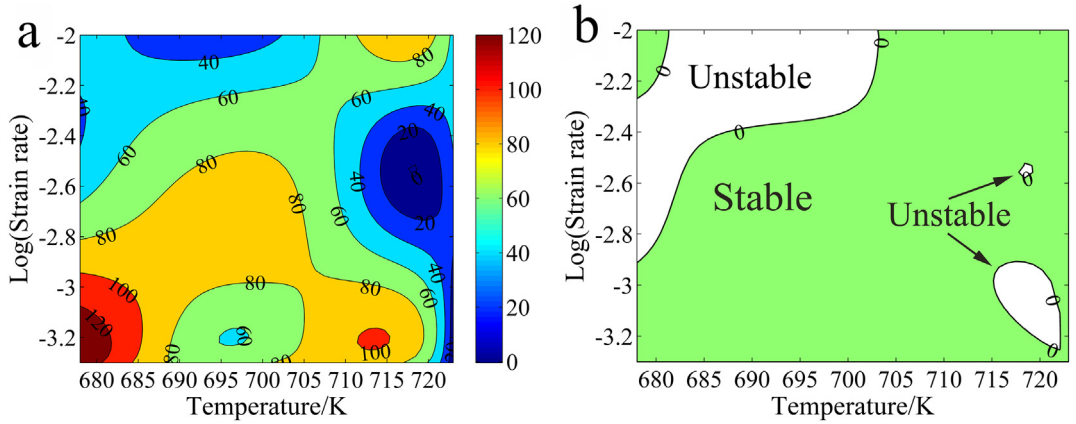

Fig. 7. Energy dissipation map (a) and flow instability map (b) of $Zr_{61.88}Cu_{18}Ni_{10.12}Al_{10}$ alloy.

exhibited a similar shape of the letter 'N' as a whole in the deeply SCLR. With the increase of temperature, the surface profiles of the specimens were gradually replaced by a shape like a drum. The transformation of these two shapes means that the alloy samples undergo a process from non-uniform to uniform rheology.

(4) The results of the processing map indicate that the optimum hot processing region of $Zr_{61.88}Cu_{18}Ni_{10.12}Al_{10}$ alloy is 688 K–708 K with a low strain-rate and 708 K–723 K with a high strain-rate.

Acknowledgments

This work was support by the National Natural Science Foundation of China (Grant No. 51661016, No. 51571105, No. 51551101, No. 51661017, No. 51661015), Wenzhou public welfare science and technology project (G20170019) and The Natural Science Foundation of Gansu Province (Grant No. 145RJZA090, No. 1606RJZA050).

References

[1] C. Yang, L.-M. Lu, Z.-W. Zhao, J.-H. Li, F. Gong, J. Ma, Micro thermoplastic forming of a Pd-based metallic glass: theory and applications, J. Iron Steel Res. Int. 24 (2017) 378–384.
[2] S. Gravier, G. Kapelski, M. Suéry, J.-J. Blandin, Thermoplastic forming of bulk metallic glasses, Int. J. Appl. Glas. Sci. 3 (2012) 180–187.
[3] J.J. He, N. Li, N. Tang, X.Y. Wang, C. Zhang, L. Liu, The precision replication of a microchannel mould by hot-embossing a Zr-based bulk metallic glass, Intermetallics 21 (2012) 50–55.
[4] G. Kumar, P. Neibecker, Y.H. Liu, J. Schroers, Critical fictive temperature for plasticity in metallic glasses, Nat. Commun. 4 (2013) 1536.
[5] N. Li, Y. Chen, M.Q. Jiang, D.J. Li, J.J. He, Y. Wu, L. Liu, A thermoplastic forming map of a Zr-based bulk metallic glass, Acta Mater. 61 (2013) 1921–1931.
[6] Y. Liu, J.J. Blandin, G. Kapelski, M. Suéry, High temperature deformation of a $Cu_{40}Zr_{44}Ag_8Al_8$ bulk metallic glass, Mater. Sci. Eng. A 528 (2011) 3748–3753.
[7] J. Schroers, Processing of bulk metallic glass, Adv. Mater. 22 (2010) 1566–1597.
[8] F. Spaepen, A microscopic mechanism for steady state inhomogeneous flow in metallic glasses, Acta Metall. 25 (1976) 407–415.
[9] Y. Zhu, G. Liao, T. Shi, M. Li, Z. Tang, F. Xiong, Thermoplastic deformation and structural evolutions in nanoimprinting metallic glasses using molecular dynamics analysis, J. Non-Cryst. Solids 427 (2015) 46–53.
[10] Y.C. Chen, J.P. Chu, J.S.C. Jang, C.W. Wu, Thermoplastic deformation and micro/nano-replication of an Au-based bulk metallic glass in the supercooled liquid region, Mater. Sci. Eng. A 556 (2012) 488–493.
[11] N. Li, X. Xu, Z. Zheng, L. Liu, Enhanced formability of a Zr-based bulk metallic glass in a supercooled liquid state by vibrational loading, Acta Mater. 65 (2014) 400–411.
[12] T. Waniuk, J. Schroers, W.L. Johnson, Timescales of crystallization and viscous flow of the bulk glass-forming Zr-Ti-Ni-Cu-Be alloys, Phys. Rev. B 67 (2003).
[13] H.J. Jun, K.S. Lee, Y.W. Chang, Deformation behavior and formability of a Ti–Zr–Ni–Be bulk metallic glass within supercooled liquid region, Intermetallics 18 (2010) 1537–1543.
[14] M.H.G. Kumar, High strain rate thermoplastic demolding of metallic glasses, Scr. Mater. 123 (2016) 140–143.
[15] B.S. Supriya Bera, Micro-patterning by thermoplastic forming of Ni-free Ti-based bulk metallic glasses, Mater. Des. 120 (2017) 204–211.
[16] A. Inoue, Stabilization of metallic supercooled liquid and bulk amorphous alloys, Acta Mater. 48 (2000) 279–306.
[17] Y.H. Liu, G. Wang, R.J. Wang, D.Q. Zhao, M.X. Pan, W.H. Wang, Super plastic bulk metallic glasses at room temperature, Science 315 (2007) 1385–1388.
[18] L. Zhang, Q. Chen, L. Liu, Deformation behavior and constitutive equation for $Zr_{55}Cu_{30}Al_{10}Ni_5$ bulk metallic glass in supercooled liquid, Acta Metall. Sin 45 (2009) 450–454.
[19] T.G. Nieh, J. Wadsworth, C.T. Liu, T. Ohkubo, Y. Hirotsu, Plasticity and structural instability in a bulk metallic glass deformed in the supercooled liquid region, Acta Mater. 49 (2001) 2887–2896.
[20] A.V.D. Beukel, On the kinetics of structural relaxation in metallic glasses, Key Eng. Mater. 81-83 (1993) 3–16.
[21] W.H. Wang, The Nature and Properties of Amorphous Matter, (2013).
[22] W.J. Kim, D.S. Ma, H.G. Jeong, Superplastic flow in a $Zr_{65}Al_{10}Ni_{10}Cu_{15}$ metallic glass crystallized during deformation in a supercooled liquid region, Scr. Mater. 49 (2003) 1067–1073.
[23] G. Wang, J. Shen, J.F. Sun, Y.J. Huang, J. Zou, Z.P. Lu, Z.H. Stachurski, B.D. Zhou, Superplasticity and superplastic forming ability of a Zr–Ti–Ni–Cu–Be bulk metallic glass in the supercooled liquid region, J. Non-Cryst. Solids 351 (2005) 209–217.
[24] J. Zhou, Z. Li, J. Zhang, F. Tian, A. Numerical Computation, Method for hot processing map based on Matlab, Chin. J. Rare Met. 31 (2007) 49–52.
[25] Y.V.R.K. Prasad, H.L. Gegel, S.M. Doraivelu, J.C. Malas, J.T. Morgan, K.A. Lark, D.R. Barker, Modeling of dynamic material behavior in hot deformation: forging of Ti-6242, Metall. Trans. A. 15 (1984) 1883–1892.
[26] S.V.S.N. Murty, B.N. Rao, On the development of instability criteria during hot-working with reference to IN 718, Mater. Sci. Eng. A 254 (1998) 76–82.